

Structure of an Early Intermediate in the M-State Phase of the Bacteriorhodopsin Photocycle

Marc T. Facciotti,^{*} Shahab Rouhani,[†] Fredrick T. Burkard,[†] Felicia M. Betancourt,[†] Kenneth H. Downing,[†] Robert B. Rose,[‡] Gerry McDermott,^{§¶} and Robert M. Glaeser^{*†‡§}

^{*}Graduate Group in Biophysics, [†]Life Sciences Division, Lawrence Berkeley National Laboratory, [‡]Department of Molecular and Cell Biology, Stanley/Donner ASU 3206, [§]Physical Biosciences Division, Lawrence Berkeley National Laboratory, [¶]Macromolecular Crystallography Facility, Advanced Light Source, Lawrence Berkeley National Laboratory, University of California, Berkeley, California 94720 USA

ABSTRACT The structure of an early M-intermediate of the wild-type bacteriorhodopsin photocycle formed by actinic illumination at 230 K has been determined by x-ray crystallography to a resolution of 2.0 Å. Three-dimensional crystals were trapped by illuminating with actinic light at 230 K, followed by quenching in liquid nitrogen. Amide I, amide II, and other infrared absorption bands, recorded from single bacteriorhodopsin crystals, confirm that the M-substate formed represents a structure that occurs early after deprotonation of the Schiff base. Rotation about the retinal C13—C14 double bond appears to be complete, but a relatively large torsion angle of 26° is still seen for the C14—C15 bond. The intramolecular stress associated with the isomerization of retinal and the subsequent deprotonation of the Schiff base generates numerous small but experimentally measurable structural changes within the protein. Many of the residues that are displaced during the formation of the late M (M_N) substate formed by three-dimensional crystals of the D96N mutant (Luecke et al., 1999b) are positioned, in early M, between their resting-state locations and the ones which they will adopt at the end of the M phase. The relatively small magnitude of atomic displacements observed in this intermediate, and the well-defined positions adopted by nearly all of the atoms in the structure, may make the formation of this structure favorable to model (simulate) by molecular dynamics.

INTRODUCTION

Bacteriorhodopsin (bR), a membrane protein from *Halobacterium salinarum*, uses light energy to generate a proton-motive force across the cell membrane (Stoeckenius, 1999). After photon absorption by the retinal chromophore, five spectroscopically characterizable intermediates (designated K, L, M, N, and O) are formed in sequence, followed by a return to the resting state, bR₅₆₈ (Lozier et al., 1975). In the M-state phase of this photocycle there appear to be at least three substates whose visible spectra show little difference, but which can be distinguished by their infrared spectra, by their nuclear magnetic resonance spectra, and by other physical measurements (for review, see Betancourt and Glaeser, 2000).

Understanding the molecular biophysics by which light energy creates a proton-motive force requires high-resolution crystal structures for each of the key intermediates and their major substates. Considerable progress has already been made in this direction. Electron diffraction experiments of two-dimensional crystals of wild-type and various mutants have provided medium resolution models for some of the conformational changes (Subramaniam et al. 1999, 2000; Vonck, 2000) that occur during the photocycle. These studies suggest that some relatively large structural movements occur during the photocycle, but they lack the de-

tailed information (e.g., side-chain displacements and water molecule positions) that high-resolution models can provide. After the discovery that the lipidic cubic phase provides a medium suitable for the growth of well-ordered crystals of bR (Landau and Rosenbusch, 1996), the resting state (bR₅₆₈) (Luecke et al., 1999a), the K-state (Edman et al., 1999), the late M-states formed by the D96N mutant (Luecke et al., 1999b) and the wild-type protein (Sass et al., 2000), and an early M-state species formed by the E204Q mutant (Luecke et al., 2000) have been modeled. A model of the L-intermediate has also been published (Royant et al. 2000), but we will not make detailed comparisons with this model because of the controversy that exists over the spectroscopic characterization of intermediates that were contained in these crystals (Balashov and Ebrey, 2001).

We now report an x-ray crystallographic determination of the structure of an early M-state intermediate of wild-type bR, formed by illumination at 230 K. This study has been undertaken to extend earlier electron diffraction work in which the M-state was trapped by a similar protocol (Hendrickson et al., 1998). As in the previous work, infrared spectroscopy has been used to characterize the particular substate of the M-intermediate that is trapped by illuminating at low temperature. In the current work, however, use of an infrared microscope was needed to obtain spectra from single crystals of bR that were grown in the monoolein gel.

The structure of the early M intermediate obtained in this work provides an informative snapshot in the sequence of conformational changes that occur between the resting state and the later M-state structures. The retinal chromophore in our early M intermediate has moved further toward the

Received for publication 8 June 2001 and in final form 23 August 2001.

Address reprint requests to Robert M. Glaeser, Lawrence Berkeley National Laboratory 363 Donner Laboratory, Berkeley, CA 94720. Tel.: 510-642-2905; Fax: 510-486-6488; E-mail: rmglaeser@lbl.gov.

© 2001 by the Biophysical Society

0006-3495/01/12/3442/14 \$2.00

cytoplasmic side of the membrane than is the case immediately after isomerization, i.e., in the K-intermediate, but not as far as in the late M state. Only a few of the movements of residues reported for the late M substate are already completed in our early M substate, some have not yet begun to occur, and some are between their resting (bR_{568}) position and that which they adopt in late M.

The three water molecules that participate in hydration of the complex counter ion on the extracellular side of the protein have reorganized in our early M structure to a configuration similar to that previously reported for the early and late M substates formed by the E204Q (Luecke et al., 2000) and D96N (Luecke et al., 1999b) mutant proteins, respectively, in which only one well-ordered water remains in that vicinity. This reorganization seems likely to occur coincident with the deprotonation of the Schiff base, i.e., the step that defines the L-to-M transition. The reorganization of R82 and the associated waters is similar to that seen in the E204Q mutant early M but with one difference in the area of this side-chain substitution, i.e., the addition of a water, corresponding to water 1717 in the wild-type late M (Sass et al. 2000), nestled in an alcove created particularly by the side chains of residues E194 and E204. In addition, we also find evidence for a water molecule on the cytoplasmic side of the protein, corresponding to water molecule 503 modeled by Luecke et al. (2000). Although there is little direct evidence for waters 501 and 504 in our wild-type early M structure, cavity calculations using VOIDOO (Kleywegt and Jones, 1994) reveal voids that are large enough to contain these water molecules at their E204Q-mutant, M-state coordinates. This indirect evidence suggests that water 501 and 504 may occupy their respective cavities in our wild-type early M intermediate, but that they are nevertheless too disordered to be modeled with reasonable B factors.

An important goal of structural studies such as these should be to both guide and validate realistic calculations of the forces that determine the trajectory of bR's cascade down its energy landscape early in the photocycle. We believe that the structural changes observed in our early M structure, together with the series of states immediately before and after it, may represent a progression of steps that are sufficiently close to one another, that physical calculations can track the transition from one to the next.

MATERIALS AND METHODS

Crystallization

Purple membrane was isolated from cells of *Halobacterium salinarum* (Oesterhelt and Stoerkenius, 1974) and solubilized by room-temperature incubation in 1.2% octylglucoside (OG) dissolved in 0.025 M Na/K phosphate buffer, pH 5.6. After 24 h, unsolubilized material was removed by ultracentrifugation at $150,000 \times g$ for 30 min. The solubilized protein was then concentrated to 18 mg/ml by use of Amicon Centricon 30 tubes (Millipore, Bedford, MA).

Individual crystallization conditions were set up in 200- μ l polymerase chain reaction tubes. Approximately 13 mg of 1-monoleoyl-*rac*-glycerol (MO) (Sigma, St. Louis, MO) was weighed into each tube, and concentrated protein solution was added to the tube in the ratio 1 μ l of solubilized protein per mg of MO. The tubes were then centrifuged at 22°C for 10 min each at speeds corresponding to $6000 \times g$, $7000 \times g$, $8000 \times g$, $9000 \times g$, and $10,000 \times g$, respectively, rotating the tubes by 180° between each step. The tubes were finally centrifuged for 100 min at $10,000 \times g$ and then once more for 3 h at $10,000 \times g$, again rotating them by 180° between each step. No other steps were taken to achieve uniform distribution of protein within the hydrated gel, and indeed large variations in protein concentration can be seen throughout the gel when the tubes are examined in a dissecting microscope. Current work indicates that the series of centrifugation steps can be simplified and reduced considerably without affecting the final result. After centrifugation the tubes were allowed to stand overnight at $21^\circ\text{C} \pm 1^\circ\text{C}$, after which dry buffer salt was added to the tubes and the samples were again centrifuged at 22°C for 3 h at $10,000 \times g$. Buffer salt was prepared for each tube by drying 6 μ l of 0.5 M Na/K-phosphate buffer, pH 5.6, for each microliter of solubilized bR that had been added to the dry MO. Hexagonal plates of bR are easily detected within 1 week, and grow to a size of $\sim 70 \mu\text{m}$ or more over the period of one to two months. Crystallization also seemed to be facilitated by overlaying the gel with 100 μ l of 2% OG in 3.0 M Na/K-phosphate buffer, pH 5.6. After crystal growth, small aliquots of the crystallization trials were scooped from the polymerase chain reaction tubes with the flat tip of a gel-loading pipette tip and allowed to soak in a liberating solution of 3.0 M Na/K-phosphate, pH 5.6, 1% OG (Luecke et al. 2000) until individual crystals could be harvested. The detergent concentration should be visibly above its cloud point in the high phosphate solution, and if it is not, the salt concentration should be raised.

Trapping and characterization of the early M intermediate

A custom-built workstation has been constructed to trap intermediate states in the bR photocycle. Crystals that were candidates for x-ray diffraction data collection were mounted on cryoloops (Hampton Research, Laguna Niguel, CA), frozen in liquid nitrogen, and illuminated for 3 min at 230 K with light from a mercury-vapor microscope lamp (Olympus, Tokyo), filtered by a Schott OG515 glass filter. Fig. 1 shows a schematic diagram of the design of this workstation. The cryoloop, whose base is held by a magnet at the end of the sample rod, was first withdrawn from the liquid nitrogen bath and positioned within the controlled temperature chamber. The chamber itself was cooled by a continuous purge of cold nitrogen gas whose temperature, as measured by a probe mounted inside the chamber, was controlled by regulating the rate of nitrogen boil off in the supply dewar. When the temperature was at the desired value, the crystal was illuminated from below, while a window at the top of the chamber was used to observe the change in color of the crystal. After the crystal had been illuminated at the desired temperature, the shutter between the chamber and the liquid nitrogen bath was again opened, and the sample was rapidly quenched in the liquid nitrogen. The cryoloop was then removed from the end of the sample rod and kept in a standard storage dewar until used for x-ray diffraction data collection. Except for the step in which the sample is illuminated with yellow light, all operations (including mounting and aligning the crystal on the goniometer of the diffraction camera) were carried out with the lowest practical level of light intensity.

Samples in the bR_{568} resting state were simply frozen and held at liquid nitrogen temperature without being "processed" in the workstation. Control samples (mock-illuminated samples) were identically processed but without actinic illumination after warming to 230 K. It is important to emphasize that those samples that were processed in the workstation were first frozen and then warmed up to the desired temperature. This protocol minimizes the danger of dehydrating the sample in the cold nitrogen stream during cool down.

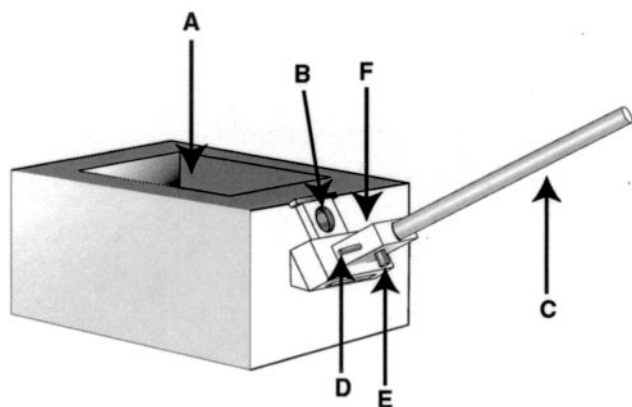


FIGURE 1 Schematic drawing of the workstation used for trapping bR crystals in the early M substate of the photocycle. Protein crystals, mounted on cryoloops and frozen in liquid nitrogen, are originally placed into the tank of liquid nitrogen (A) to which is attached a small chamber, shown on the right. The sliding shutter (B) separates the chamber from the tank when in the “up” position, as shown in the figure, but allows the rod (C) to pass through into the liquid nitrogen tank when pushed into the “down” position. This arrangement allows one to mount a crystal at the end of the rod (C) under liquid nitrogen and bring it into the chamber. The shutter is then closed, and the temperature is brought up to the desired value by adjusting the flow rate of nitrogen being boiled off from a storage dewar chamber (by way of the tubing indicated schematically by D). When the sample is at the desired temperature, it is illuminated by light brought in through a flexible light pipe, indicated schematically by the cylinder E at the bottom of the chamber. A window at the top of the chamber (F) allows observation of the crystal with a microscope, if desired, to confirm the change in color from purple to yellow. After illumination, the shutter is again opened, and the rod is rapidly pushed down into the liquid nitrogen, thereby quenching the sample and permanently trapping the photocycle intermediate that is formed during illumination.

Single crystals of bR that were illuminated at 230 K were also characterized by infrared spectrophotometry. An epi-illumination infrared microscope (Spectra-Tech Nic-Plan, Spectra-Tech, Shelton, CT) located on beam line 1.4 at the Lawrence Berkeley National Laboratory Advanced Light Source was used for this purpose. By recording spectra from only the region of a uniformly thick crystal, not including any of the surrounding MO gel, we were able to avoid the severe absorption flattening that occurs in spectra of inhomogeneous samples, as was evident in an earlier, time-resolved study of the M-state spectrum of bR crystals (Heberle et al., 1998). Spectra were obtained from areas 20 μm in diameter with a Nicolet Magna 760 infrared spectrophotometer (Nicolet, Madison, WI). Samples of MO gel containing thin crystals were sandwiched between a polished copper substrate and a 6-mm-diameter calcium fluoride window, using a compressed rubber gasket to seal the window tightly to the substrate to avoid dehydration of the sample. The sealed sample was then cooled under vacuum with a model U-320 Joule-Thompson refrigerator (MMR Technologies, Mountain View, CA). Because of the relatively slow cooling rate of this sample holder (~ 10 min required to cool from ambient to 230 K), the surrounding MO gel transforms to a turbid phase when cooled to low temperature (Rummel et al., 1998; Ai and Caffrey, 2000). Nevertheless, samples could be made in which the amount of MO gel lying above and below the bR crystal was thin enough that this turbidity had no noticeable effect on the spectra obtained in the area of the crystal. Formation of the M intermediate in the photocycle was again accomplished by illuminating the sample at 230 K for 3 min with light filtered through the Schott OG515 glass filter described above. Fourier transform infrared (FTIR) data were collected before and then immediately after illumination as a series of 256

scans, each requiring 1 s to complete, yielding spectra with a resolution of 4 cm^{-1} . Between each such run the samples were warmed to 298 K and illuminated with white light for 30 s before cooling again in the dark to repeat the cycle. The FTIR difference spectrum presented in Fig. 3 is the average of six such runs.

Diffraction data collection and analysis

X-ray diffraction data were collected at beam line 5.0.2 at the Lawrence Berkeley National Laboratory Advanced Light Source. A 100- μm pinhole collimator was used for these crystals, and the samples were held at a temperature of 100 K. Data were collected on the Quantum IV CCD camera (Area Detector Systems Corporation, Poway, CA) as 1° rotation images. The HKL suite of programs (Otwinowski and Minor, 1997) was used to convert the CCD camera data to background-subtracted diffraction intensities. Exposure times ranged from 10 to 30 s per frame. Data quality remained good in the highest resolution zones after 80 or 90 frames, although some reduction of diffraction intensity in the outer-resolution shells could often be observed at the end of the series, due to radiation damage (Glaeser et al., 2000). Data were collected for several crystals each of the resting state, the mock-illuminated control, and the early M state obtained by illumination at 230 K. The work reported here describes only the results obtained for the crystal of each type, which exhibited the best resolution and data statistics. Whereas data of the quality reported for the mock-illuminated crystal can be obtained quite routinely, that reported for the resting-state crystal is encountered only rarely. The slightly poorer resolution and greater mosaicity encountered with crystals trapped in the M state reflects a constant postillumination trend for crystals selected from the same tube.

All crystals of the M-intermediate showed some discoloration after recording ~ 15 x-ray diffraction images, even though they had still appeared by eye to be pure yellow in color after mounting and alignment was completed. The crystals eventually developed a stable, rusty orange color well before any significant effect of radiation damage could be noticed in the quality of the high-resolution data, a phenomenon that had been described to us previously by Hartmut Luecke (personal communication). The purple crystals (the resting state samples and the mock-illuminated samples), on the other hand, showed no visible changes in color as a result of exposure to the x-ray beam. We suspect that the development of a rusty orange color is due to some reprotonation of the Schiff base that occurs as a result of radiation damage.

Crystallographic refinement was carried out with SHELX-97 (Sheldrick and Schneider, 1997). The coordinates for 1C3W (Luecke et al., 1999a) from the protein data bank (PDB) were taken as the starting model for the refinement of the ground state and mock-illuminated state. The coordinates for 1C3W (Luecke et al., 1999a) and 1C8S (Luecke et al., 1999b) were used as starting models for two independent refinements of the early M structure. It should be noted that no starting models used for refinement contained the chromophore, lipid, or water molecules of their parent models. The progress of refinement was monitored by following changes in R_{free} , which was calculated with 7% of the measured data for the resting state and the M-state data sets and with 5% of the data for the mock-illuminated data set. Although all data specified in Table 1 were used during refinement, the values of R and R_{free} cited in the text are those calculated with reflections for which $F > 4\sigma$. We further adopt the unconventional practice of reporting the R values that have been multiplied by the square root of 2, so that the number reported can be compared directly with R values that are typically obtained from crystals of proteins that do not suffer from twinning. This practice is noted in the text by quoting numerical values divided by the square root of 2, whereas in Table 1 the rows are explicitly labeled “ R factor $\times \sqrt{2}$.” As has been explained by Redinbo and Yeates (1993), the R values for crystals that are twinned in a nearly 50:50 ratio are smaller by a factor of the square root of 2 relative to an equivalent, untwinned crystal. This convention has not been adopted for previously reported structures, and this fact should be accounted for

TABLE 1 Refinement statistics

Statistics	Ground state	Mock trapped	Early M intermediate
Data reduction			
Unit Cell (Å) a,b	60.99	60.886	60.745
c	109.13	109.591	108.240
Resolution range (Å)	1.65–20	1.8–20	2.0–20
Unique structure factors	26,695	20,519	14,618
Mosaicity (°)	0.5	0.5	0.8
Average $I/\sigma(I)$ all data/highest resolution shell	32.8/3.2	26.1/5.2	20/3.0
Completeness (%) all data/highest resolution shell	98.7/96.8	97.5/99.7	95/90
R_{merge} (%) all data/highest resolution shell	3.6/35.8	5.0/41.0	5.0/45.0
Refinement Statistics			
Number of structure factors	25,672	19,440	13,408
Number of restraints	9755	7418	7152
Number of parameters	8819	7348	6955
Twin ratio	51:49	50:50	51:49
Number of protein atoms	1720	1714	1668
Number of retinal atoms	20	20	20
Number of water molecules	27	22	13
Number of lipid atoms	283	79	37
R factor $\times \sqrt{2}$ (%) data $F > 4\sigma(F)$ /all data	17.7/18.4	22.1/23.3	22.2/23.7
R free $\times \sqrt{2}$ (%) data $F > 4\sigma(F)$ /all data	25.3/26.6	29.3/30.0	29.0/30.7
Average protein B (Å ²)	26.1	31.0	29.4
Average retinal B (Å ²)	19.0	24.4	20.6
Average water B (Å ²)	33.1	38.5	36.9
Average lipid B (Å ²)	54.1	47.8	46.3
Deviation from ideal bond lengths (Å)	0.017	0.007	0.008
Deviation from ideal bond angles (deg.)	0.034	0.020	0.022

$R_{\text{merge}}(I) = \frac{\sum_{\text{hkl}} \sum_i |I_{\text{hkl},i} - \langle I_{\text{hkl}} \rangle|}{\sum_{\text{hkl}} \sum_i I_{\text{hkl},i}}$, where $\langle I_{\text{hkl}} \rangle$ is the average intensity of the multiple $I_{\text{hkl},i}$ observations for symmetry-related reflections. $I/\sigma(I)$, average of the diffraction intensities, divided by their standard deviations.

R factor = $\frac{\sum_{\text{hkl}} |F_o - F_c|}{\sum_{\text{hkl}} |F_o|}$, where F_o and F_c are observed and calculated structure factors, respectively.

R free = $\frac{\sum_{\text{hkl}} |F_o - F_c|}{\sum_{\text{hkl}} |F|}$, where the summation is restricted to structure factors of a test set, which was selected in thin-resolution shells to avoid twinning bias.

when comparing model quality. In so doing, however, one must also note that “adjustment” of published R values will require less than the factor of the square root of 2 used here, if data have been collected from crystals that are not as fully twinned as those that we could find in our work.

One model that we initially used for refinement of the M-state data set allowed for two conformations of the protein. The first conformation was that of the high-resolution structure for the mock-illuminated protein, whose occupancy, $(1 - f)$, was allowed to vary but whose parameters were constrained to be those of the unilluminated control. The second conformation was that of the early M state itself, of occupancy f , for which all parameters were allowed to vary as in the previous refinement of the resting state and the mock-illuminated state. The fraction of M (i.e., the parameter f) always increased during refinement, even when the initial value was set to be 0.98, and the value of f was found to increase more rapidly during refinement the smaller the initial value of this parameter. We thus concluded that the occupancy of the M state was very close to 100%, and the final stages of refinement were carried out with $f = 1$.

As noted earlier, two independent starting models, 1C3W and 1C8S, were used for refinement to determine how sensitive the final result would be to modest differences in the starting model. The atomic coordinates of the resulting two refined structures exhibited a root mean square coordinate difference (rmsd) of 0.45 Å. Differences in atomic position that are greater than 3σ are largely confined to either side-chains in loops or those on the membrane exposed surface. All lipid and water molecules in the two models were also identical. Consistent with these similarities, the two models produced values of R_{free} that differed by less than 0.3%. The following analysis of the structure of early M is based upon the model with the lower R_{free} , which corresponds to the refinement based upon 1C8S as the starting model.

Model structures were rebuilt manually a number of times during refinement to minimize spatially correlated (i.e., nonrandom) features in the $F_o - F_c$ map, but changes made during rebuilding were only accepted as long as they reduced the value of R_{free} . OMIT maps and the programs OOPS (Kleywegt and Jones, 1996) and PROCHECK (Laskowski et al., 1993) were also used to identify parts of the structures that might need manual adjustment. In addition, we found that manual reduction in the B factors of some regions of the main chain was able to eliminate continuous strands of density that existed previously in some regions of the $F_o - F_c$ map when contoured at 3σ .

Carbon atoms 5 to 13, 18, 19, and 20 in the retinal group were restrained but not constrained to be planar in both the all-*trans* and 13-*cis* conformations. Permitting unrestrained rotation of the bonds in the retinal group to allow modeling of a more highly twisted conformation in the early M intermediate did not improve the value of R_{free} .

Average values for the coordinate errors that are given in Table 2 were estimated from Luzzati plots, a procedure that tends to overestimate the magnitude of the error (Brunger, 1997). These estimates were nevertheless

TABLE 2 Luzzati plot values

Model	Luzzati coordinate error (Å)
Ground state	0.11
Mock trapped	0.17
Early M intermediate	0.15

used as a conservative criterion to decide whether differences in atomic positions that are modeled for two structures are significantly larger than expected from the estimated error in the coordinates. A value of 3σ , in which σ is the Luzzati estimated coordinate error, is used as the low cutoff value for determining whether the rmsd between equivalent atoms or residues in two structures being compared represents a significant difference in position. An rmsd greater than 3σ is considered a significant movement, whereas an rmsd less than 3σ is considered to be within experimental error.

During the early phases of refinement, water molecules were added to the model structures by enabling the SWAT command in SHELXL. This instruction allows SHELXL to automatically devine reasonable water molecules according to Babinet's principle (Sheldrick and Schneider, 1997). In later stages of refinement $F_o - F_c$ maps, contoured to as low as 2.7σ , were also used for placing water molecules. Candidate water molecules were retained in the final model only if their B factor remained smaller than 60 after refinement. After the process of refinement was judged to be sufficiently complete, the program VOIDOO (Kleywegt and Jones, 1994) was used to probe for cavities at positions of water molecules that were reported in other models but which we do not see with a reasonable B factor in our early M structure. Initial trials at locations where our refined structure did contain a well-defined water molecule demonstrated that an initial grid size of 0.25 Å and a probe radius of 1.1 Å was required to identify a cavity where a water molecule really existed. These settings were then used to probe a small grid centered on the coordinates of the water molecule in question.

Figs. 3 through 7 were drawn using MolMol (Koradi et al., 1996). Fig. 8 was generated using programs in the CCP4 suite (Collaborative Computational Project, 1994).

RESULTS

Data collection and refinement statistics are summarized in Tables 1 and 2. All crystals used in this study were twinned in a nearly 50:50 ratio (Luecke et al., 1998), although in other work, not reported here, we have encountered crystals for which the minor twin fraction was as low as 17%.

The bR₅₆₈, resting-state structure

The structure of the bR₅₆₈ resting state obtained by refinement against our 1.6-Å resolution data set is very similar to that of the starting model, 1C3W (Luecke et al., 1999a). The overall rmsd are 0.307 Å, α -carbon backbone only, and 0.380 Å, all protein atoms. The positions of all water molecules reported by Luecke et al. (1999a), with the exception of water 414 near the extracellular surface of the protein, are confirmed in our structure. Additionally, five new water molecules numbered 421, 422, 423, 515, and 516 were also modeled. All lipids modeled in 1C3W, with the exception of squalene, could be fit to density and their coordinates refined with acceptable B factors. There are, nevertheless, a few differences between our refined structure and the previously published structure from which our refinement began. Most of the significant differences, greater than 3σ , are confined to residues in loops and those at the cytoplasmic end of helix F.

Positive densities located at the positions of hydrogen atoms in many of the H bonds of the 1.6-Å resolution $F_o - F_c$

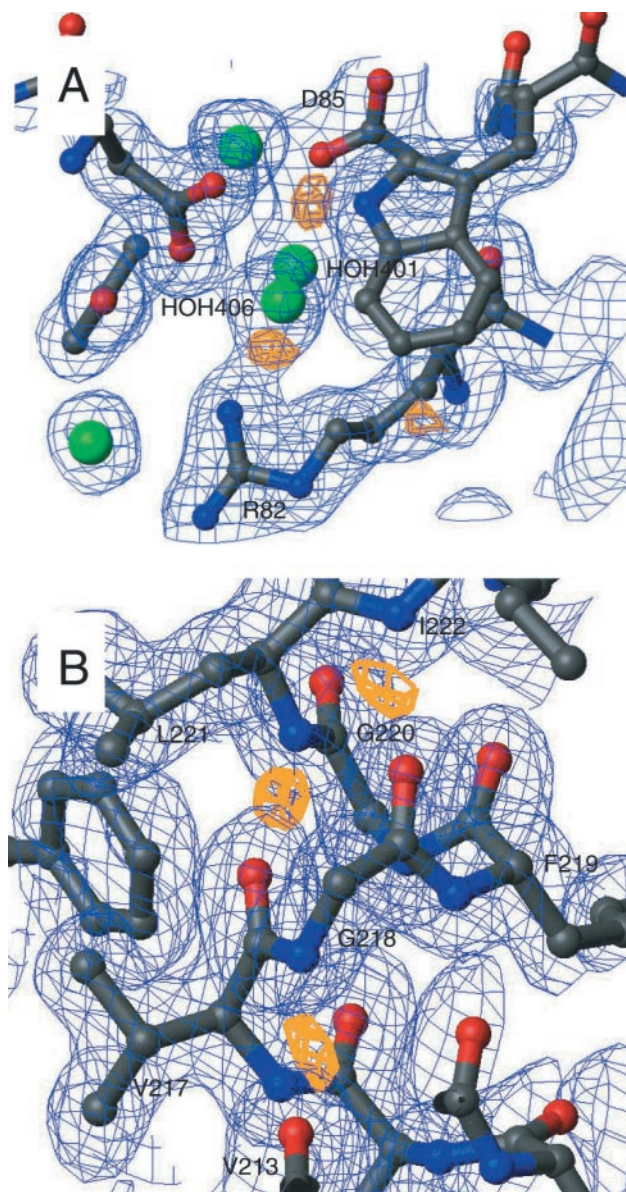


FIGURE 2 Two examples of the positive difference peaks observed between H-bond donors and H-bond acceptors in the $F_o - F_c$ difference map of the bR resting-state structure, contoured at 3σ and painted yellow. In blue, the $2F_o - F_c$ map is contoured at 1.2σ . (A) Waters 401 and 406 are hydrogen bonded to residues D85 and R82, respectively. Positive $F_o - F_c$ peaks can be seen in the region of the hydrogen bond. There is also a positive $F_o - F_c$ noise peak near the base of the side chain of R82. (B) A region of helix G showing a helical arrangement of positive difference peaks midway between the amide nitrogen atoms and the carbonyl oxygen atoms.

F_c map of the resting-state sample (Fig. 2), contoured at 3σ , were an unexpected feature that emerged in the later stages of refinement. These densities are not accompanied by negative densities on the opposite side of the adjacent H-bond donor or acceptor atoms, ruling out the possibility that the densities are a result of incorrect placement of the donor or acceptor atoms. When anisotropic B factors were

introduced for the associated H-bond donor and acceptor atoms, R_{free} dropped from $26.1/\sqrt{2}$ to $25.8/\sqrt{2}$, but the densities within the H bonds were not significantly affected. We therefore conclude that the densities seen within these H bonds are not an artifact that results from representing anisotropic atomic vibration by an isotropic B factor. The positive densities could be greatly reduced, and often eliminated, by including hydrogen atoms on the H bond donors, using restraints provided within SHELX-97. The addition of 55 such H atoms further reduced the value of R_{free} to $25.5/\sqrt{2}$.

Mock-illuminated control

The refined structure of the mock-illuminated control is, with only a few exceptions, very similar to that of the resting state. The rmsd between the mock-illuminated control structure and that of the resting state is 0.179 Å for all backbone atoms and 0.305 Å for all atoms. Of the small structural changes that occur as a result of equilibrating the crystal at 230 K (in the dark), the most significant are the loss of interpretable density for residue 162 at the cytoplasmic end of helix F and a 52° rotation around Chi-3 of residue E194 that results in a 1.47-Å displacement of OE1. Other differences are also found on residues 32, 41, 56, 74, 164, and 166 (adjacent to the disordered end of helix F). All nine of the internal water molecules present in the resting state could be found in the mock-illuminated state. Lipid residues 612, 613, and parts of 602, 604, 605, 606, 607, 609, and 610 from 1C3W could be modeled into density, and their atomic coordinates refined with acceptable B factors.

Early M state intermediate

The infrared difference spectrum shown in Fig. 3, recorded from single crystals of bR after illuminating the sample at 230 K, exhibits the prominent negative peak at 1527 cm^{-1} that is seen in the L, M, and N intermediates, all of which contain the retinal in the 13-*cis* configuration. Although the positive amide II peak ($\sim 1550\text{ cm}^{-1}$) is much stronger than it is in the L-state intermediate, the negative, C = N (Schiff base) band at 1640 cm^{-1} is very strong whereas the negative amide I peak ($\sim 1660\text{ cm}^{-1}$) is weak, as they are in IR spectra of the L intermediate (Hendrickson et al., 1998; Ormos et al., 1992; Hessling et al., 1993). It thus seems likely to us that the yellow-colored species trapped in these three-dimensional crystals represents an early, L-like substate of the M-intermediate in which the protein-structural changes have nevertheless gone beyond those that are present in the L intermediate, as is indicated by the pronounced peak in the amide II band.

Refinement of the initial model structure, 1C8S, against the diffraction data obtained from a crystal trapped in the early M state resulted in numerous structural changes that

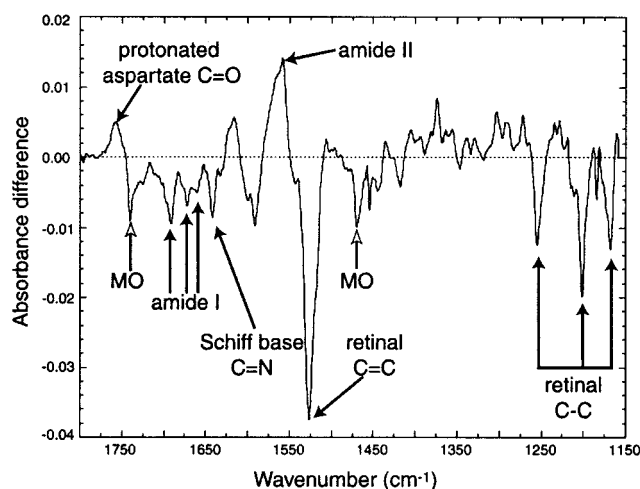


FIGURE 3 FTIR difference spectrum between the M state and the resting state of wild-type bR, recorded at 230 K from a single crystal grown within the mono-olein cubic phase. Six pairs of spectra (unilluminated and illuminated specimens, respectively; 256 scans each) were recorded between 1800 and 1100 cm^{-1} . For each pair, an illuminated-minus-unilluminated difference spectrum was calculated, and the spectrum shown is the average of these. Difference peaks associated with the amide I and II modes of the peptide backbone are identified by closed arrows. The positions of the absorbance maxima for vibrational modes of some other important chemical groups, including those arising from the isomerization of retinal, are denoted by simple lines. Open arrowheads indicate difference peaks associated with strong absorption bands of the mono-olein gel medium; the cause of this light-induced change is unknown at present.

are not seen in the mock-trapped crystal. For instance, residues 162 to 166 in the EF loop, modeled in the ground state, are too disordered to be modeled in the early M structure. In addition, although the majority of the protein backbone positions do not change significantly, more than 50 of the side chain residues (i.e., over 20% of the total protein) move by distances greater than 3σ . Many of the most significant movements that do occur are concentrated around the E204 cavity and the retinal-binding pocket on the extracellular side of the protein. Residues 167 to 175 were too disordered to be modeled in the late M formed by three-dimensional crystals of the D96N mutant. However, clear difference density features in our $F_o - F_c$ maps indicated that these residues had remained ordered in our early M. These residues were thus rebuilt manually. Finally, only lipids 612, 613, and part of 602 could be built into density.

The largest displacement of a protein-residue from its position in the mock-illuminated state is a 4.6 Å movement of NH1 of residue R82. This displacement causes a reorganization of water molecules, two of which we have assumed to be waters 403 and 406. What we believe to be water 406, but which we have renumbered 409 to be consistent with the E204Q early M model, continues to form a hydrogen bond with NH2 of Arg-82, although water 409 is now displaced by 4.85 Å. What we believe to be water 403 is displaced by

5.75 Å and now forms new hydrogen bonds with OE1 of E194 and the backbone nitrogens of residues 193 and 194 in a binding alcove lined with residues of the extracellular ends of helices F and G and the FG loop.

A water molecule, corresponding to water 503 in the E204Q mutant early M intermediate, is found on the cytoplasmic side of the chromophore in our early M model. Whereas there is no direct evidence in our electron density map for waters 405 and 504, VOIDOO provides evidence for cavities large enough to accommodate these molecules. In addition, despite weak electron density features near a position in which water 501 could expect to be found, the B factor of a water molecule refined to occupy this density feature rapidly soars above our cutoff value of 60. Cavity calculations using VOIDOO again reveal a cavity in this location that is large enough to contain a water molecule. This indirect evidence suggests that water 501 could occupy that cavity, but that if it does, this water molecule is nevertheless too disordered in our early M structure to model with a reasonable B factor.

Comparison of the early M substate with other models

As we compare various features in the early M and late M structures, we have chosen to show only the late M model obtained with the D96N mutant protein (i.e., 1C8S) in figures that illustrate the points under discussion. This choice reflects our concern that the wild-type late M model (1CWQ) is derived from crystals in which it is estimated that multiple intermediates (resting state, early M, and late M) share significant degrees of occupancy. This multiple occupancy reduces the amount of signal arising from the desired (late) M intermediate and complicates the data analysis due to the presence of competing signal from other species. We are thus inclined to place greater weight on the structure that was trapped with the D96N protein. In addition, the comparison discussed here has been made with revised coordinates deposited in the PDB for 1F4Z. The coordinate file originally deposited for 1F4Z was, by mistake, not the file that represented the final refinement of the structure, nor did it correspond to the configuration of R82 illustrated in Fig. 5 *a* of Luecke et al. (2000). We thank Dr. Hartmut Luecke for clarifying this discrepancy and for providing the correct coordinate file, which has since been deposited in the PDB. The refined structure reported by Luecke et al. (2000), as is now shown by the PDB entry differs from 1F4Z as originally deposited only in the side-chain of R82 and by the addition of water 409 in place of water 552.

Many of the structural rearrangements seen in our wild-type early M intermediates are similar to those seen in previous models of bR M intermediates. It is nevertheless clear, when we compare our early M model to the late M models, that some of the residues, which have moved in the

late M models, have remained in their mock-illuminated positions in our early M structure. Furthermore, many of the other residues that move by a significant amount in the late M intermediates seem to have moved to intermediate positions in our early M model.

Fig. 4 shows that structural movements involving D85, the Schiff base, and the 13-*cis* retinal are all similar, but different in magnitude, to those noted for the late M and early M states (Luecke et al. 1999b, 2000; Sass et al. 2000). The displacement of the D85 side chain that we obtain is not as large as the movement of the D85 side chain of the E204Q mutant M intermediate or wild-type late M, but it is larger than that reported for the D96N mutant late M. The plane of the side-chain carboxyl group of D85 has rotated only slightly in our early M structure, but nevertheless the distance from OD1 of D85 to OG1 of T89 increases from 2.7 to 3.7 Å, effectively breaking this hydrogen bond.

As is true for previously refined models of the M-state species (Luecke et al. 1999b, 2000; Sass et al. 2000), our crystallographic refinement is thus in disagreement with the interpretation made by Kandori et al. (2001) for their measurements of the decreased and increased 2502 cm⁻¹ and 2463 cm⁻¹ IR bands, respectively. We suggest that a full calculation of the potential energy surface for this particular vibrational mode, based on existing x-ray crystal structures, may be required to resolve the apparent inconsistency between the x-ray and infrared data.

The isomerized retinal chromophore in our early M model has moved to a position between that found in the ground state and that which it adopts in D96N late M, as is also true in the E204Q-mutant. As a consequence of this relatively small displacement toward the cytoplasmic side, the side chain of W182, which is in steric contact with the methyl group of carbon 13, is only slightly displaced in our early M. This displacement can be characterized as being similar to that seen in the E204Q mutant M intermediate and far less than is seen in either of the late M intermediates. The relatively large movement of Trp-182 reported in a structure meant to be the L intermediate (Royant et al., 2000) is greater than what we find in the early M state, implying that the movement seen in the “L structure” should really be attributed to the partial occupancy of a 412-nm absorbing (“M”) species in those crystals, and further implying that the contaminating species is more like the late M state than it is like our early M state.

Nuclear magnetic resonance experiments have suggested that the Schiff base C=N bond may be highly strained in the L intermediate and that this strain is progressively released in the transition through the M phase of the photocycle (Hu et al., 1998). In accord with this suggestion, we find that the torsion angle of the bond between C14 and C15 of the retinal chromophore is significantly greater in the early M structure than it is in the models of the late M intermediate. Whereas the ground-state and mock-illuminated state C14—C15 torsion angles are respectively 4 and

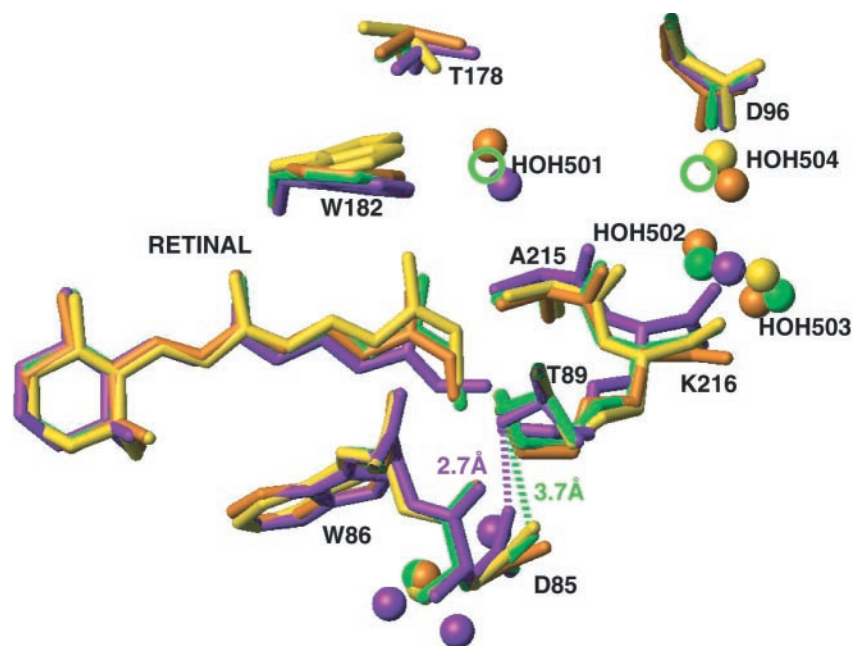


FIGURE 4 A view almost perpendicular to the axis of the retinal group, showing the three progressive positions occupied by this group and various other residues in the resting configuration (*purple*); as trapped in our early M substate (*green*); in the position adopted by the 204Q mutant early M substate 1F4Z (*orange*), and in the position ultimately adopted in the late M structure, 1C8S (*yellow*). Note that labels on water molecules are shown with the same color as their respective model if they occupy unique positions, whereas water molecules that appear at the same position in multiple models have been labeled in black. Open circles indicate cavities detected by VOIDOO in the early M intermediate structure, for which waters that are present in other models could not be modeled in our early M structure with reasonable B factors.

5.8° away from an ideally planar conformation, the C14—C15 torsion angle in wild-type early M intermediate is 26°, and it is reduced to 13.6° in the mutant D96N late M (Luecke et al., 1999b). We also note that the coordinates deposited for the published model of the K intermediate (Edman et al., 1999) show a C14—C15 torsion angle of only 4.2°, whereas the coordinates deposited by Royant et al. (2000) for a model thought to be the L intermediate show a torsion angle of only 1.2°. Torsion about the C14—C15 bond in the K-intermediate cannot be excluded on the basis of the published model, as Edman et al. (1999) constrained the retinal backbone and Schiff base linkage (including CZ of K216) to be planar in the 13-*cis*, 15-*anti* configuration. The nature and occupancy of intermediates in crystals used for the L intermediate model are controversial, as noted above, and in addition, no information was provided about the use of constraints during the refinement in that case. We can also mention that the C14—C15 torsion angle is reduced to 3.3° in the late M structure reported for wild-type bR (Sass et al., 2000), but in doing so we again express our reservations about the more complicated data analysis problem that had to be dealt with in refining this model structure.

Internal water molecules are seen to be quite active in the transition to the early M state, as is illustrated by the examples shown in Figs. 4 and 5. Whereas water molecules 404 and 407 remain fixed in place, waters 401, 402, and 406 are rearranged and are replaced by a single water molecule

(identified as 401). Water 409, which we propose may have been water 406, appears in the site previously occupied by NH₂ of residue R82 in its ground-state position. Water 409 is hydrogen bonded to NE and NH₂ of R82 when it is in its early M position. The configuration of the side chain of R82 is similar to that found for R82 in the E204Q mutant, early M intermediate. In our early M structure, water 501 is neither bound in its ground/mock-illuminated-state position between NE of W182 and the carbonyl oxygen of A215 nor is it found in a position similar to that of the E204Q early M structure (where it is bound between OG of T178 and NH of W182) (Luecke et al., 2000). In addition, water 502 moves by 1.68 Å to make room for water molecule 503, which is hydrogen bonded to the cytoplasmic side of the carbonyl oxygen of K216. Although we do not have direct evidence that either water 501 or water 504 are present in our early M model, there are two pieces of indirect evidence that suggest both could still be present. The first evidence to cite is the fact that cavity calculations describe one void, large enough to accommodate a single water molecule, encompassing the two positions found for water 501 in the ground state and the E204Q early M state, respectively, and a second void centered at the coordinates for water 504 of the E204Q model. The second point is that the ground-state hydrogen bond between OG of T46 and OD1 of D96 is broken in our early M model. This is an event for which the energy cost can be kept low by the insertion of a water molecule, as does

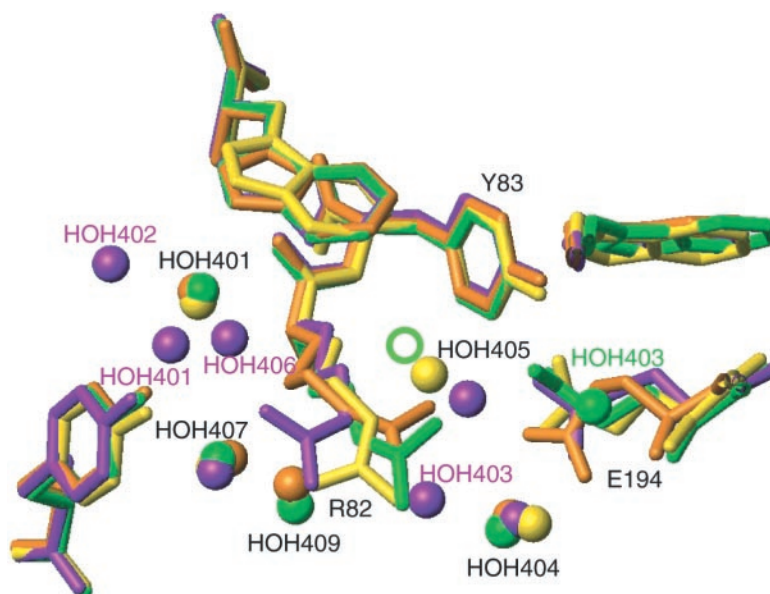


FIGURE 5 Residues in the region of R82 are shown for each of the four states shown in Fig. 4. The same color and labeling schemes have been adopted for this figure, as were described in the legend for Fig. 4.

indeed happen in the E204Q early M structure (Luecke et al. 2000). The configuration of internal water molecules in our wild-type, early M intermediate is thus similar to that found in the E204Q mutant M-intermediate and wild-type late M intermediate.

Fig. 6 shows one area in which there are some differences between our early M intermediate and the intermediates formed by the D96N or E204Q mutants. The guanidinium group of R82 in our early M, wild-type intermediate, is in a position that lies between those modeled for the D96N mutant and the E204Q mutant M-states, corresponding to a more substantial displacement than was reported for the D96N late M intermediate but one that is not as large as that modeled in the wild-type late M intermediate by Sass et al. (2000). The movement associated with the change in the side-chain position of R82 is additionally propagated along the backbone from residue 82 through residue 84 and is similar, but not as large, as the movement reported in this region of helix C by Royant et al. (2000). In addition, residues E194 and E204 are modeled with slightly different positions for our early M than are reported for either mutant M structure. A comparison of these two residues in the wild-type early M and wild-type late M structures reveals that residue E204 also adopts very distinct positions in these two cases, whereas the position of E194 is very similar (data not shown). Fig. 7 shows our refined model for this same area of the wild-type, early M structure, indicating various hydrogen bonds that are formed between adjacent side chain groups and with internal water molecules. Of note is a water, which we presume to be water 403, analogous to water 1717 in the wild-type late M, hydrogen bonded to

OE1 of E194 and the amide backbone nitrogens of residues 193 and 194 (see also Fig. 6 for these details).

We were especially curious to know whether the structural changes observed as a result of our x-ray crystallo-

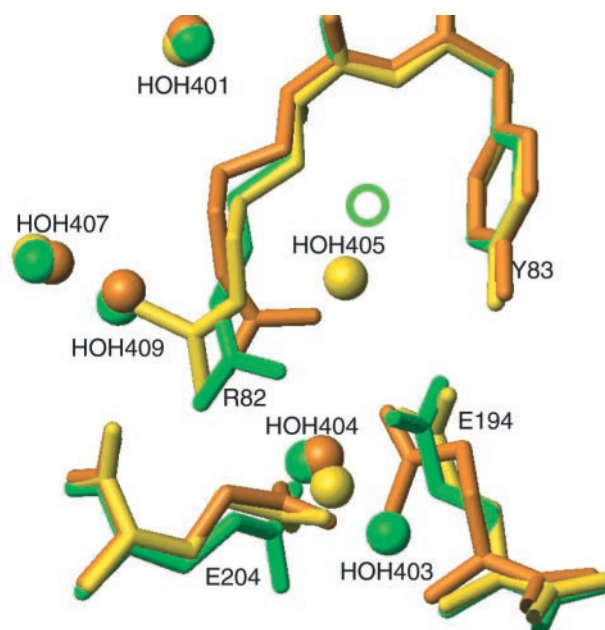


FIGURE 6 A comparison of the side chain positions for R82 and other nearby residues in the wild-type early M (green), the E204Q mutant early M (orange), and the D96N mutant late M (yellow). Water molecules are shown as spheres with the same color coding. The green circle for water 405 indicates the presence of a "cavity" that could accommodate a water molecule.

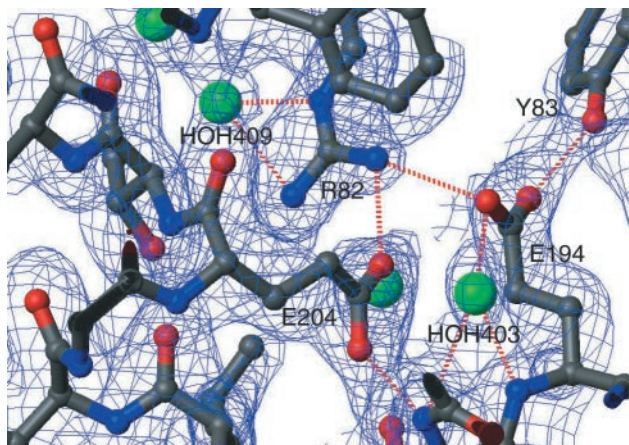


FIGURE 7 Residues Y83, R82, E194, E204, and waters 403 and 409 in their wild-type early M configuration. The electron density map is a $2F_o - F_c$ map contoured at 1.2σ . Hydrogen bonds are drawn with dashed red lines.

graphic refinement would produce a difference Fourier projection map similar to that observed in our earlier electron diffraction experiments (Hendrickson et al., 1998). The experimental x-ray structure amplitudes could not be used to compute projection maps for such a comparison because the space group of the x-ray crystals is different from that of the native, two-dimensional crystals, and in addition the x-ray crystals are highly twinned. The resolution was intentionally restricted to the interval between 15 and 3.5 Å to correspond to that used for our electron-diffraction difference maps (Hendrickson et al., 1998). The atomic coordinates for our refined crystal structures were therefore transferred to the P3 space group and aligned to the coordinates of the electron crystallographic model of bR (2BRD) before calculating projection maps of the x-ray structures.

A direct comparison of projection maps for the resting state of bR, shown in Fig. 8, reveals that the projected electron diffraction and x-ray diffraction density maps differ from one another by more than has previously been recognized. Fig. 8 A shows the resting state projection map calculated from experimental electron structure factors, whereas Fig. 8 B shows the corresponding projection map calculated from the atomic model that was obtained by refinement against the x-ray diffraction data. Although a few high-resolution features in the two projection maps show close correspondence to each other, the differences between them (especially in the region of helices F, G, and A) are, for the most part, much greater than the differences that could occur between the resting state and the M-intermediate. Quantitative characterization of the factors explaining the differences shown in Fig. 8, A and B, lies outside the scope of the present paper. We only note that a number of factors could contribute: 1) the alignment of the x-ray structure to 2BRD may not give the direction of projection as accurately as desired due to inevitable errors in

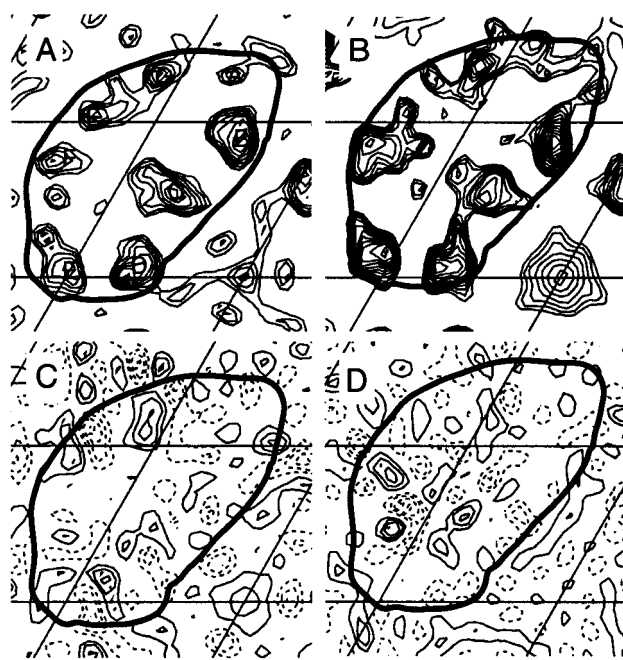


FIGURE 8 Comparison of projection maps that are based upon electron diffraction studies with two-dimensional crystals (A and C) and x-ray diffraction studies with three-dimensional crystals (B and D). (A) Electron-diffraction projection-map of the light-adapted resting state of bR (redrawn from Hendrickson et al., 1998). (B) Corresponding projection map calculated for the mock-illuminated state that is obtained from our refined x-ray crystal structure. (C) Electron-diffraction difference-Fourier map obtained from two-dimensional crystals that were converted to the M state by illumination at 230 K (redrawn from Hendrickson et al., 1998). (D) The difference-Fourier projection-map calculated from the refined models of our early M substate and the mock-illuminated control sample. The x-ray projection maps are calculated with structure factors between 15 and 3.5 Å resolution to be comparable with those calculated for two-dimensional crystals from electron diffraction data (Hendrickson et al., 1998). Using the program O, selected α -carbon atoms from both the mock-illuminated and early M state models were used to calculate a least-squares best fit to the respective α -carbons in 2BRD. The resulting alignment matrix was then applied to all atoms of both the mock-illuminated and early M models before structure factors were calculated for the two models.

the electron diffraction model having been built at a lower resolution. 2) The contribution that hydrogen atoms make to electron scattering is considerable, whereas their contribution to the x-ray projection has been ignored. Thus, in principle, the two projection maps should look somewhat different. 3) The experimental electron diffraction amplitudes are affected by the atomic B factors, which are larger toward the membrane surfaces for the two-dimensional crystals than they are in the three-dimensional crystals. Whereas each of these points could be investigated in some detail, we have elected not to pursue the question further as a part of the present study.

Despite the rather large, quantitative differences that exist between our x-ray and electron projection-maps it has nevertheless been demonstrated that major features observed in

both x-ray and neutron difference Fourier projection maps remain qualitatively similar to those exhibited in electron difference Fourier projection maps. We have therefore calculated the difference Fourier projection map for our early M atomic model, and it is shown in Fig. 8 D.

There are no prominent difference peaks similar to those seen in electron diffraction studies of the M_N -intermediate produced by the D96N mutant protein (Subramaniam et al., 1993), by the triple mutant in which the protein is constitutively in the cytoplasmically open conformation (Subramaniam et al., 1999), and even in maps derived from x-ray (Koch et al., 1991; Nakasako et al., 1991; Sass et al., 1997) and neutron diffraction (Dencher et al., 1989) experiments with purple membrane films, under conditions that favor accumulation of a late M or M_N intermediate. Even the weaker peaks observed in wild-type M that was trapped at 230 K, shown again in Fig. 8 C, are not present in the current x-ray difference map. The absence of strong difference peaks at locations expected for a late M (or even M_N -like) intermediate, and the absence of even the weaker peaks observed in the electron diffraction difference map for an intermediate trapped at 230 K, thus supports the idea that this x-ray structure describes a very early, almost L-like intermediate in the photocycle. We have also drawn this same conclusion, as is mentioned above, from the infrared spectrum of three-dimensional crystals that are converted to the M intermediate by illumination at 230 K.

DISCUSSION

It seems inevitable that the photoisomerization of the retinal group places new, unbalanced stresses on the previously stable, resting state structure of bR. A full understanding of how bR functions as an electrogenic pump thus requires that the foci of greatest mechanical frustration be identified at each stage in the photocycle. A series of experimentally obtained, high-resolution structural snapshots can provide a valuable framework for quantitative calculations of these physical forces, which drive bR through its photocycle. If quantitative physical calculations are judged to be not yet sufficiently reliable for this purpose, we would argue that it is even more unlikely that qualitative intuition and chemical insight can nevertheless identify which structural changes represent true cause-and-effect elements of the mechanism and which are merely epiphenomena that play no mechanistic role. Accurate determination of the structure at a series of well-characterized intermediate points within the photocycle, of the type we have attempted to produce here, must therefore be coupled to the quantitative application of physical theory before one can realistically say that the molecular biophysics of this system is correctly understood.

The M substate trapped in the current work represents a relatively well-defined structure. This substate nevertheless accommodates a disordered ensemble of conformations of residues 162 to 166 on the cytoplasmic side of helix F, the

first of which is already disordered before the sample is illuminated, and an ensemble of states with either poorly ordered or empty sites for several of the internal water molecules. For most of the atoms in the protein, however, one can think of our early M structure as identifying a well-defined local minimum along the photocycle pathway, one that is readily accessible at 230 K but from which the protein cannot easily escape in either the forward or backward direction at that temperature. The well-defined nature of this intermediate structure should thus make it a favorable one to include in calculations that seek to identify the principal sites of physical stress that determine the photocycle trajectory.

The relatively low values for B factors that have been obtained for the majority of protein atoms in this atomic model encourages us to think that the M state structure that has been trapped with our protocol represents a unique and well-defined structural state. We note that the good value of R_{free} tells us that this must certainly be the case to the same extent that is true for any protein structure that is obtained by x-ray crystallography. We consider this to be an important point because the radiation-induced discoloration of bR crystals, which started initially in a yellow (M) state, could indicate that one or more non-M species are produced by a mechanism not unlike the blue-light-induced return of M to the bR resting state. As noted in the Materials and Methods section, we suppose that this discoloration does, indeed, result in the formation of one or more protonated Schiff-base species. As this supposed reprotonation happens at a specimen temperature of 100 K, well below the dynamic transition temperature (Zaccai, 2000) however, we are not surprised to find little evidence of accompanying dual (or multiple) occupancy of alternative protein structures.

The local minimum in free energy in which our early M state structure is trapped might be much deeper at 230 K than it is at ~ 290 K. It would seem that this must be the case, because the early M species (substates) are believed to be in rapid equilibrium with the L intermediate at room temperature (Varo and Lanyi, 1991). The L-to-M (forward) rate does not itself become very slow until the sample is cooled to ~ 170 K. The M-to-L (backward) rate could thus only be made appreciably slower than the forward rate (i.e., the value of the equilibrium constant could only be changed) if the depth of the local minimum for the early M state is, itself, temperature dependent. Among the molecular explanations that might account for the apparent temperature dependence of the depth of this local minimum, one can point to the obvious differences that occur in water activity (i.e., availability of liquid or at least highly mobile water) at a temperature well below the freezing point. In considering why the early M species is accumulated at such high occupancy, it may again be significant to note that the temperature at which this early M substate is trapped is close to the dynamical transition temperature of bR (Zaccai, 2000), i.e.,

the temperature below which anharmonic (i.e., large-amplitude) motions within the protein can no longer occur.

The slight differences in structure between our wild-type early M and that of the E204Q mutant may be largely due to the obvious chemical differences between the carboxyl and carbamoyl groups of the aspartate and asparagine side chains, respectively. It may be possible, for instance, that water 403 in our early M cannot be bound in the E194/Q204 alcove of the E204Q mutant early M due to the mutation-induced change in the local electrostatic field, and the resulting differences in position of the side chains of other residues near this alcove. Another formal possibility is that the intermediates trapped by the wild-type and mutant proteins represent distinctly different, sequential substates of the M intermediate. Regardless of the interpretation it is nevertheless encouraging to find that introducing the E204Q substitution seems to have little other effect, even locally, on the protein component of the structural changes seen in the photocycle. This observation supports the validity of using site-direct mutants of bR in structural studies of photointermediates. The quantitative (MD calculation) analysis of the progression between various photocycle intermediates will also benefit from requiring that these simulations should quantitatively capture the subtle differences that are seen in the two cases.

It should be noted that crystal-packing forces may restrain the type of structural changes that the protein has access to in the three-dimensional crystals, relative to those that are accessible in the native purple membrane. The ~ 60.6 Å lattice constant within the (a, b) plane of the three-dimensional crystals is ~ 2 Å smaller than the 62.4 Å (Glaeser et al., 1985) lattice constant in the two-dimensional (purple membrane) crystals. This closer packing of trimers might limit the ability of helix F to tilt into the lipid-filled space between trimers, a point that was already recognized by Vonck (2000) as a problem for trapping the N state at high occupancy in the two-dimensional, native-membrane crystals. In addition, there are protein-protein contacts between surface loops, connecting successive layers along the *c* axis of the three-dimensional crystals, which are absent in the native membrane. The postillumination trend of increased mosaicity and decreased resolution, noted in the section above on data collection and analysis, further suggests that stress is, indeed, being applied against crystal-packing forces during formation of the M intermediate. Nevertheless, the photocycle kinetics of bR in the three-dimensional crystals, as measured by FTIR spectroscopy (Heberle et al., 1998), are only slightly altered from that of bR in the native purple membrane.

A greater steric hindrance in the three-dimensional crystals (relative to membrane sheets) may explain the fact that the structural changes we are able to see in samples trapped at 230 K are different from those seen in native membrane sheets, both in projection maps and in the three-dimensional model of a constitutively “open” triple mutant (Subrama-

niam and Henderson, 2000). The influence of steric hindrance in the three-dimensional crystals may also account for the fact that the E204Q mutant is trapped at a much earlier point in the photocycle when it is in the three-dimensional crystals than is the case in two-dimensional membrane crystals (Luecke et al. 2000). Because crystal-packing restraints may limit the change in structure that can occur within the three-dimensional crystals, it may prove to be important to include these restraints, as well as the relatively low water activity within the space between layers, when attempting to quantitatively model the changes in structure that occur at different stages of the photocycle.

Apart from the qualifications stated above concerning the nonnative environment of the protein, the coordinates and B factors resulting from refinement of the early M structure can be regarded as being highly reliable. We have shown that the structure presented here is relatively free of model-dependent bias in that the overwhelming majority of the refined parameters converge to the same values from two clearly different starting points. The care that we have taken in refinement has even been rewarded by the fact that the 1.6 Å, $F_o - F_c$ map of the resting-state protein shows positive densities for the hydrogen atoms in more than 50 of the H bonds within the structure. The inclusion of a mock-illuminated sample in this study has made it possible to recognize that the major structural changes we see in the early M structure must be attributed to intramolecular stresses generated by the isomerization of the polyene chain, and to the subsequent deprotonation of the Schiff base, rather than to just the thermal cycling that is required as part of our trapping protocol.

In general, the structural changes that occur during formation of the early M intermediate are concentrated around 1) the Schiff-base, 2) the side chain residues involved in the complex counter ion (and the proton release group), and 3) the associated (internal) water molecules. These movements precede structural changes within the cytoplasmic side of the protein that are known to occur later in the photocycle, e.g., in the formation of the N intermediate, but which are not yet characterized in as much atomic detail (Vonck, 2000). Nevertheless, even at the stage of the early M intermediate, a key hydrogen bond (between T46 and D96) is broken on the cytoplasmic side of the protein, setting the stage for larger changes that will first open, and then subsequently close, a half channel on the cytoplasmic side. Once this has all occurred, further structural changes apparently occur that open the extracellular half channel during the formation of an O-like state (S. Rouhani-Manshadi, J. P. Cartailier, M. T. Facciotti, P. Walian, R. Needleman, J. K. Lanyi, R. M. Glaeser, H. Luecke, submitted manuscript). Finally, the protein is restored to its resting-state configuration when water 402 is positioned between the protonated Schiff-base and the carboxyl group of D85. Because the carboxyl group of D85 again becomes deprotonated in this step, placement of water 402 at this site is an event that can

be interpreted as the binding of an hydroxyl ion at the extracellular "active-site position" of the ion pump followed by the immediate abstraction of a proton from the previously neutral carboxylic acid.

We thank both Dr. Ehud Landau and Dr. Jurg Rosenbusch for generously sharing advice and information on their experience in crystallizing bR within the MO cubic phase, shortly after publication of their first paper on this new method. We also thank Dr. Hartmut Luecke for extensive advice regarding the use of SHELX-97 for refinement with data obtained from the twinned bR crystals. We thank Dr. James Holton for frequent help and advice throughout the refinement of the structures presented here. Dr. Leonid Brown, Dr. Richard Henderson, Dr. Hartmut Luecke, Dr. Sriram Subramaniam, and Dr. Janos Lanyi have contributed several valuable comments on a draft of this paper. Diffraction data were obtained on beam line 5.0.2 at the Lawrence Berkeley National Laboratory Advanced Light Source, and we thank all of the staff there for their support and assistance. We are grateful to Dr. Michael Martin for invaluable assistance in the purchase and construction of the cold stage for the infrared microscope at beam line 1.4 of the Lawrence Berkeley National Laboratory Advanced Light Source, as well as for advice on numerous aspects of the infrared measurements in general.

This work was supported by the National Institutes of Health Program Project grant GM51487 and National Institutes of Health training grant GM08295.

REFERENCES

- Ai, X., and M. Caffrey. 2000. Membrane protein crystallization in lipidic mesophases: detergent effects. *Biophys. J.* 79:394–405.
- Balashov, S. P., and T. G. Ebrey. 2001. Trapping and spectroscopic identification of the photointermediates of bacteriorhodopsin at low temperatures. *Photochem. Photobiol.* 73:453–462.
- Betancourt, F., and R. M. Glaeser. 2000. Chemical and physical evidence for multiple functional steps comprising the M state of the bacteriorhodopsin photocycle. *Biochim. Biophys. Acta.* 1460:106–118.
- Brunger, A. T. 1997. Free R Value: Cross-Validation in Crystallography, in *Methods in Enzymology*. R. M. Sweet and C. W. Carter, Jr., editors. Academic Press, New York. 366–396
- Collaborative Computational Project, Number 4. 1994. The CCP4 suite: programs for protein crystallography. *Acta Crystallogr. D.* 50:760–763.
- Dencher, N., D. Dresselhaus, G. Zaccai, and G. Buldt. 1989. Structural changes in the bacteriorhodopsin during proton translocation revealed by neutron diffraction. *Proc. Natl. Acad. Sci. U.S.A.* 86:7876–7879.
- Edman, K., P. Nollert, A. Royant, H. Belrhali, E. Pebay-Peyroula, J. Hajdu, R. Neutze, and E. M. Landau. 1999. High-resolution x-ray structure of an early intermediate in the bacteriorhodopsin photocycle. *Nature.* 401: 822–826.
- Glaeser, R. M., M. Facciotti, P. Walian, S. Rouhani, J. Holton, A. MacDowell, R. Celestre, D. Cambrie, and H. Padmore. 2000. Characterization of conditions required for x-ray diffraction experiments with protein microcrystals. *Biophys. J.* 78:3178–3185.
- Glaeser, R. M., J. S. Jubb, and R. Henderson. 1985. Structural comparison of native and deoxycholate-treated purple membrane. *Biophys. J.* 48: 775–780.
- Heberle, J., G. Buldt, E. Koglin, J. P. Rosenbusch, and E. M. Landau. 1998. Assessing the functionality of a membrane protein in a three-dimensional crystal. *J. Mol. Biol.* 281:587–592.
- Hendrickson, F. M., F. Burkard, and R. M. Glaeser. 1998. Structural characterization of the L-to-M transition of the bacteriorhodopsin photocycle. *Biophys. J.* 75:1446–1454.
- Hessling, B., G. Souvignier, and K. Gerwert. 1993. A model-independent approach to assigning bacteriorhodopsin's intramolecular reactions to photocycle intermediates. *Biophys. J.* 65:1929–1941.
- Hu, J. G., B. Q. Sun, M. Bizounok, M. E. Hatcher, J. C. Lansing, J. Rapp, P. J. Verdegem, J. Lugtenburg, R. Griffin, and J. Herzfeld. 1998. Early and late M intermediates in the bacteriorhodopsin photocycle: a solid-state NMR study. *Biochemistry.* 37:8088–8096.
- Kandori, H., Y. Yamazaki, Y. Shichida, J. Raap, J. Lugtenburg, M. Belenky, and J. Herzfeld. 2001. Tight Asp-85-Thr-89 association during the pump switch of bacteriorhodopsin. *Proc. Natl. Acad. Sci. U.S.A.* 98:1571–1576.
- Kleywegt, G. J., and T. A. Jones. 1994. Detection, delineation, measurement and display of cavities in macromolecular structures. *Acta Crystallogr. Sect. D. Biol. Crystallogr.* 50:178–185.
- Kleywegt, G. J., and T. A. Jones. 1996. Efficient rebuilding of protein structures. *Acta Crystallogr. Sect. D. Biol. Crystallogr.* 52:829–832.
- Koch, M. H., N. A. Dencher, D. Oesterhelt, H. J. Plöhn, G. Rapp, and G. Büldt. 1991. Time-resolved X-ray diffraction study of structural changes associated with the photocycle of bacteriorhodopsin. *EMBO J.* 10: 521–526.
- Koradi, R., M. Billeter, and K. Wüthrich. 1996. MOLMOL: a program for display and analysis of macromolecular structures. *J. Mol. Graphics.* 14:51–55.
- Landau, E. M., and J. P. Rosenbusch. 1996. Lipidic cubic phases: a novel concept for the crystallization of membrane proteins. *Proc. Natl. Acad. Sci. U.S.A.* 93:14532–14535.
- Laskowski, R. A., M. W. MacArthur, D. S. Moss, and J. M. Thornton. 1993. PROCHECK: a program to check the stereochemical quality of protein structures. *J. Appl. Crystallogr.* 26:283–291.
- Lozier, R. H., R. A. Bogomolni, and W. Stoeckenius. 1975. Bacteriorhodopsin: a light-driven proton pump in *Halobacterium halobium*. *Biophys. J.* 15:955–962.
- Luecke, H., H. T. Richter, and J. K. Lanyi. 1998. Proton transfer pathways in bacteriorhodopsin at 2.3 angstrom resolution. *Science.* 280: 1934–1937.
- Luecke, H., B. Schobert, J. P. Cartailler, H. T. Richter, A. Rosengarth, R. Needleman, and J. K. Lanyi. 2000. Coupling photoisomerization of retinal to directional transport in bacteriorhodopsin. *J. Mol. Biol.* 300: 1237–1255.
- Luecke, H., B. Schobert, H. T. Richter, J. P. Cartailler, and J. K. Lanyi. 1999a. Structure of bacteriorhodopsin at 1.55 Å resolution. *J. Mol. Biol.* 291:899–911.
- Luecke, H., B. Schobert, H. T. Richter, J. P. Cartailler, and J. K. Lanyi. 1999b. Structural changes in bacteriorhodopsin during ion transport at 2 angstrom resolution. *Science.* 286:255–261.
- Nakasako, M., M. Kataoka, Y. Amemiya, and F. Tokunaga. 1991. Crystallographic characterization by X-ray diffraction of the M-intermediate from the photo-cycle of bacteriorhodopsin at room temperature. *FEBS Lett.* 292:73–75.
- Oesterhelt, D., and W. Stoeckenius. 1974. Isolation of the cell membrane of *Halobacterium halobium* and its fractionation into red and purple membrane. In *Methods in Enzymology*. S. Fleischer and L. Packer, editors. Academic Press, New York. 667–678.
- Ormos, P., K. Chu, and J. Mourant. 1992. Infrared study of the L-intermediates, M-intermediates, and N-intermediates of bacteriorhodopsin using the photoreaction of M. *Biochemistry.* 31:6933–6937.
- Otwinowski, Z., and W. Minor. 1997. Processing of x-ray diffraction data collected in oscillation mode. In *Methods of Enzymology*. R. M. Sweet and C. W. Carter, Jr., editors. Academic Press. New York. 307–326.
- Redinbo, M. R., and T. O. Yeates. 1993. Structure determination of plastocyanin from a specimen with a hemihedral twinning fraction of one-half. *Acta Crystallogr. Sect. D. Biol. Crystallogr.* 49:375–380.
- Royant, A., K. Edman, T. Ursby, E. Pebay-Peyroula, E. M. Landau, and R. Neutze. 2000. Helix deformation is coupled to vectorial proton transport in the photocycle of bacteriorhodopsin. *Nature.* 406:645–648.
- Rummel, G., A. Hardmeyer, C. Widmer, M. L. Chiu, P. Nollert, K. P. Locher, I. Pedruzzi, E. M. Landau, and J. P. Rosenbusch. 1998. Lipidic cubic phases: new matrices for the three-dimensional crystallization of membrane proteins. *J. Struct. Biol.* 121:82–91.

- Sass, H. J., G. Buldt, R. Gessenich, D. Hehn, D. Neff, R. Schlesinger, J. Berendzen, and P. Ormos. 2000. Structural alterations for proton translocation in the M state of wild-type bacteriorhodopsin. *Nature*. 406:649–653.
- Sass, H. J., I. W. Schachowa, G. Rapp, M. H. Koch, D. Oesterhelt, N. A. Dencher, and G. Büldt. 1997. The tertiary structural changes in bacteriorhodopsin occur between M states: x-ray diffraction and Fourier transform infrared spectroscopy. *EMBO J.* 16:1484–1491.
- Sheldrick, G. M., and T. R. Schneider. 1997. SHELXL: High Resolution Refinement. *Methods in Enzymology*, R. M. Sweet and C. W. Carter, Jr., editors. Academic Press, New York. 319–343.
- Stoeckenius, W. 1999. Bacterial rhodopsins: evolution of a mechanistic model for the ion pumps. *Protein Sci.* 8:447–459.
- Subramaniam, S., M. Gerstein, D. Oesterhelt, and R. Henderson. 1993. Electron diffraction analysis of structural changes in the photocycle of bacteriorhodopsin. *EMBO J.* 12:1–8.
- Subramaniam, S., and R. Henderson. 2000. Molecular mechanism of vectorial proton translocation by bacteriorhodopsin. *Nature*. 406:653–657.
- Subramaniam, S., I. Lindahl, P. Bullough, A. R. Faruqi, J. Tittor, D. Oesterhelt, L. Brown, J. Lanyi, and R. Henderson. 1999. Protein conformational changes in the bacteriorhodopsin photocycle. *J. Mol. Biol.* 287:145–161.
- Varo, G., and J. K. Lanyi. 1991. Kinetic and spectroscopic evidence for an irreversible step between deprotonation and reprotonation of the Schiff base in the bacteriorhodopsin photocycle. *Biochemistry*. 30:5008–5015.
- Vonck, J. 2000. Structure of the bacteriorhodopsin mutant F219L N intermediate revealed by electron crystallography. *EMBO J.* 19:2152–2160.
- Zaccai, G. 2000. How soft is a protein? A protein dynamics force constant measured by neutron scattering. *Science*. 288:1604–1607.